Coherent GHz lattice and magnetization excitations in thin epitaxial Ag/Fe/Cr/Fe films

Derang Cao [1,2,*] Roman Adam,[2,3,†] Daniel E. Bürgler [2,3] Fangzhou Wang,[2] Chengkun Song,[4] Shandong Li,[1]
Martin Mikulics [5,3] Hilde Hardtdegen [5,3] Sarah Heidtfeld,[2] Christian Greb [2] and Claus M. Schneider[2,3,6]

[1]*College of Physics, Center for Marine Observation and Communications, Qingdao University, 266071 Qingdao, China*
[2]*Peter Grünberg Institute (PGI-6), Forschungszentrum Jülich, 52425 Jülich, Germany*
[3]*Jülich-Aachen Research Alliance (JARA), Fundamentals of Future Information Technology, 52425 Jülich, Germany*
[4]*Key Laboratory for Magnetism and Magnetic Materials of MOE, Lanzhou University, 730000 Lanzhou, China*
[5]*Ernst Ruska Zentrum (ERC-2), Forschungszentrum Jülich, 52425 Jülich, Germany*
[6]*Faculty of Physics, University Duisburg-Essen, 47057 Duisburg, Germany*
and Department of Physics, University of California Davis, Davis, California 95616-5270, USA

We excited an epitaxial magnetic Ag/Fe/Cr/Fe multilayer nonthermally and nonoptically with very short (<1 ps) electromagnetic pulses. We detected the synchronous phononic-magnetic response by time-resolved magneto-optical Kerr effect measurements. The Ag/Fe/Cr/Fe multilayer was patterned into a coplanar waveguide transmission line, and the electromagnetic pulses were generated by pulsed-laser illumination of an integrated GaAs photoconductive switch (PCS). The detected magnetic excitations comprise up to four narrow-band high-order modes with the highest frequency reaching 30 GHz. The mode frequencies are independent of both temperature in the range from 16 to 300 K and the applied external magnetic field up to 120 mT. Our analysis shows that the origin of the rigidity of these high-frequency modes is the strong coupling of the magnetic subsystem with the lattice of the Ag/Fe/Cr/Fe multilayer. The exciting electromagnetic pulse generated by the PCS induces, via magnetoelastic coupling, long-lived (ns) standing GHz acoustic waves *normal* to the Ag/Fe/Cr/Fe film plane. These lattice oscillations in turn couple back and drive the magnetization oscillations via the magnetoelastic coupling. The temperature and field dependence of the damping of the oscillations can be described by inelastic phonon-phonon and phonon-magnon scattering. Our study opens up a possibility of using coherent lattice and magnetization dynamics in ferromagnetic films for spintronic devices at GHz clock rates.

I. INTRODUCTION

The understanding and control of the interaction between electron, phonon, and spin subsystems in epitaxial thin films and multilayers is essential for the rigorous description and possible application of ultrafast phenomena driven by phonon and magnetization dynamics. The entire dynamic process involves the interaction between electrons, phonons, and spins, and therefore spin dynamics became a heavily debated and often controversial topic of modern magnetism [1–5]. This subsequently prompted an active field of research exploring new possibilities to efficiently control the spin state by employing ultrafast excitations, including phonons and magnetization excitations [2,6–8]. It has been confirmed that the angular momenta of electrons and spins interact in the form of electronic or magnonic currents [9] and that they allow electric control and detection of magnetization dynamics [10]. Recent x-ray diffraction experiments have demonstrated that the angular momentum of the spin system can be transferred to the surrounding lattice and therefore an interaction between spin and lattice plays an essential role in the ultrafast magnetization dynamics [11].

A number of experiments have previously shown that femtosecond laser pulses can trigger lattice and magnetization excitations by direct optical excitation [6,8,12]. Recently, surface acoustic waves [13] and coherent phonons [14,15] have been successfully used for exciting magnetization precession in ferromagnetic films, where the excitation of high-frequency periodic strain induces elastic waves that subsequently generate magnetization precession via magnetoelastic coupling. This indicates that the lattice oscillations can excite magnetization. Due to the magnetoelastic coupling of the magnetic subsystem with the lattice, the reverse process—the excitation of coherent phonons induced by magnetization dynamics—is in principle possible as well. Nevertheless, we note that the detection of phonons is experimentally much more difficult due to the lack of direct contrast mechanisms. A scenario of magnetization dynamics induced phonon pumping has been suggested theoretically in Ref. [16], where it was considered that phonons can be generated via magnetoelastic coupling. Experimental studies of phonon dynamics magnetoelastically coupled to the magnetic system are extremely rare [14], and thorough experiments are needed to reach more detailed physical understanding of the phonon-magnon interplay on femto- to nanosecond timescales.

*caodr@qdu.edu.cn
†r.adam@fz-juelich.de

Here we report on the observation of high-frequency narrow-band lattice oscillations coupled to a magnetic reservoir in an epitaxially grown Ag/Fe/Cr/Fe multilayer. The entire layer sequence shows excellent lattice matching confirmed by low-energy electron diffraction (LEED). We detected phononic oscillations in the GHz frequency range and their higher-order modes up to the fourth order using magnetization oscillations magnetoelastically coupled to the phonon subsystem. We stress that these phononic oscillatory modes (and the accompanying magnetic oscillations) were triggered *without* any direct optical or thermal excitation. Instead, we employed extremely short [<1 ps full width at half maximum (FWHM)] electromagnetic pulses generated by a photoconductive switch (PCS) placed at a distance over 200 μm from the targeted area as a trigger. Several previous studies report the observation of laser-induced coupled phonon and magnetization dynamics of low orders, which, in contrast to our approach, were all *induced thermally* [8,12,15]. We found in our experiment that the frequencies of all observed modes are completely independent of both temperature and magnetic field, while their amplitudes show temperature-dependent damping. These very stable and rigid phonon resonances can be both triggered and recorded due to magnetoelastic coupling in the Ag/Fe/Cr/Fe multilayer.

II. METHODS

The Ag/Fe/Cr/Fe structure was fabricated on a low-temperature grown GaAs substrate (LT GaAs). The 1 μm thick LT GaAs epitaxial film was grown on top of a 300 nm thick AlAs interlayer on a semi-insulating GaAs(001) wafer in a Varian GEN-II molecular-beam epitaxy (MBE) system. The growth process was performed at 250 °C followed by annealing at 600 °C for 10 min. The Ag/Fe/Cr/Fe(001) multilayer was deposited in another, home-built MBE system. After the transfer and the unavoidable exposure to ambient conditions, the LT GaAs substrate was first heated to 585 °C for 30 min to remove oxides and residual water vapor from the surface as checked by Auger spectroscopy. The fabrication started by depositing epitaxial Fe seed (1 nm) and Ag(001) buffer (150 nm) layers. After annealing the buffer system at 300 °C for 30 min [17], the Fe(7 nm)/Cr(0.9 nm)/Fe(3 nm) trilayer was deposited at 150 °C. All these layers have good mutual lattice matching and grow in a well-defined epitaxial manner [17]. Finally, a 3 nm thick MgO cap layer was deposited at room temperature to protect the sensitive Fe/Cr/Fe trilayer against oxidation and degradation during patterning. Following the deposition, the sample was covered with a photoresist that was subsequently patterned by optical lithography in order to define a 50-Ω coplanar waveguide (CPW) transmission line (with 100 μm central linewidth and 8 mm length) as well as an embedded metal-semiconductor-metal PCS [Figs. 1(a) and 1(b)]. Argon ion-beam etching was used to transfer the desired CPW and PCS pattern into the Ag/Fe/Cr/Fe/MgO multilayer. Photoresist removal and wire bonding concluded the fabrication process.

The setup of our time-resolved magneto-optic experiment (TR MOKE) is shown in Fig. 1(c). In order to excite the PCS and to generate electromagnetic pulses propagating along the CPW, we employed a 76-MHz train of 100-fs pulses from a
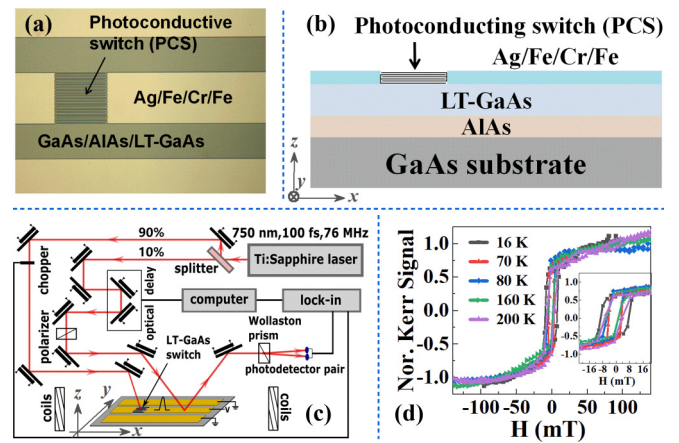

FIG. 1. Experimental setup. (a) Microscopic photograph of the Ag/Fe/Cr/Fe coplanar waveguide (CPW) with the integrated photoconductive switch (PCS). (b) Cross section of the Ag/Fe/Cr/Fe PCS structure. (c) Schematics of the experiment: An ultrafast optical pump pulse triggers the PCS to launch a current pulse into the CPW. The current pulse generates a short magnetic field pump pulse that, in turn, excites the Ag/Fe/Cr/Fe multilayer. Magnetization dynamics were traced at a distance of >200 μm from the PCS using time-resolved magneto-optical Kerr effect (TR MOKE) measurements. (d) Temperature dependence of the hysteresis loop of Fe/Cr/Fe trilayer. Inset shows details of the hysteresis around zero field.

Ti:sapphire laser (wavelength $\lambda = 750$ nm). The laser beam was first split into two optical paths with an intensity ratio of 90%–10%. The laser fundamental beam (so-called optical pump) was employed for the PCS excitation, and the much weaker, frequency-doubled beam (optical probe) was used to gently probe the magnetic state of the excited multilayer. In our TR MOKE setup, the plane of light incidence is oriented parallel to the CPW long axis and the probe light is incident at an angle of about 45 ° with respect to the surface normal. A split-coil electromagnet was used to magnetize the sample in plane and along the CPW. This geometry results in sensitivity to both the dynamic in-plane magnetization component along the CPW and the dynamic out of plane magnetization component due to the longitudinal and polar Kerr effect, respectively. The diameter of the probe beam in focus at the sample surface was slightly below 100 μm, covering almost the entire width of the central line of the CPW. The magnetic easy axes of the Fe(001) films were aligned at 45 ° with respect to the long axis of the CPW, which runs along a ⟨100⟩ direction of GaAs(001) and coincides with an ⟨110⟩ in-plane magnetic hard axis of Fe(001). The electromagnetic pulses generated by the PCS propagate along the CPW and generate magnetic field pulses with a peak amplitude of up to $B \approx 10$ mT (calculated) in the plane of the sample. The pulsed B field is in plane and perpendicular to both the external magnetic field H_{ext} and the CPW long axis. In detail, triggered by the excitation with the femtosecond laser pulse, the PCS launches a current pulse of picosecond duration along the CPW, which flows mainly in the Ag layer. The current pulse generates an Oersted field that propagates along the CPW together with the current pulse. Since the center conductor of the CPW has a large width to thickness aspect ratio of about 620 (width = 100 μm,

thickness = 161.9 nm), the field lines of the Oersted field encircle the central conductor in an extreme stadiumlike shape. Hence, the Oersted field at the position of the MOKE probing spot, which is focused to the middle of the 100 μm wide central conductor, is perpendicular to the long axis of the CPW and in the plane of the sample. The out of plane component due to the curvature of the field lines is therefore negligible. The temporal width of the generated pulses is defined by the photoexcited carrier lifetime in LT GaAs, the capacitance of the PCS, and the electromagnetic pulse dispersion along the transmission line, and results in pulses with a FWHM of about 0.6 ps as determined by electro-optic sampling in a separate experiment. The measured result is shown in Fig. S6 of the Supplemental Material [18]. These data are fully comparable with the results previously reported [19,20]. The evolution of the magnetization dynamics induced by the magnetic field pulses has been recorded in the time window up to 2000 ps by controlling the time delay between the exciting magnetic field pulse and the optical probe pulse, which is varied using a mechanical delay line with a minimum step size of 1.5 μm corresponding to a minimum increment of the time delay of 10 fs.

III. RESULTS

The magnetic hysteresis loop of the in-plane magnetization of the Fe/Cr/Fe trilayer measured at different temperatures is shown in Fig. 1(d). The shape of the curves with remanent magnetization $M_r \approx \pm 0.4 M_s$ followed by a smooth transition to saturation indicates that for applied fields (H_{ext}) lower than the coercive field (H_c) the magnetizations of the two layers are aligned along different easy axes with an intermediate angle of 90°, e.g., ⟨100⟩ and ⟨010⟩. For $H_{ext} > H_c$ the intermediate angle continuously decreases until both layer magnetizations saturate at about 100 mT along the field direction, e.g., ⟨110⟩. In Fe/Cr/Fe trilayers with a Cr thickness of about 1 nm and grown under the present conditions on an Ag(001) buffer layer, the 90° configuration in the remanent state is stabilized, because the biquadratic term of the interlayer exchange coupling and the magnetocrystalline anisotropy dominate over bilinear coupling [21]. H_c shows a slight increase with decreasing temperature from 200 down to 16 K. Typical TR MOKE signals measured at various magnetic field intensities H_{ext} in the interval between 5 and 120 mT and at constant temperature $T = 70$ K are shown in Fig. 2(a). The corresponding fast Fourier transform (FFT) spectra are displayed in Fig. 2(b). On the other hand, Figs. 2(c) and 2(d) show the experimental TR MOKE traces and the corresponding FFT spectra, respectively, measured at different temperatures T in the range from 70 to 200 K, but at constant field, $H_{ext} = 40$ mT. The FFT spectra reveal for all temperature and magnetic field dependent measurements five resonances at frequencies between 7.4 and 30.1 GHz. Notably, the frequencies of all five observed modes are practically *independent of both T and H_{ext}*. Only the f_2 mode shows a weak temperature dependence. The external field and temperature seem to affect only the *amplitudes* of the resonances. Furthermore, the damping of the oscillations appears to be independent of H_{ext} [Fig. 2(a)] but substantially decreases at low temperatures [Fig. 2(c)].
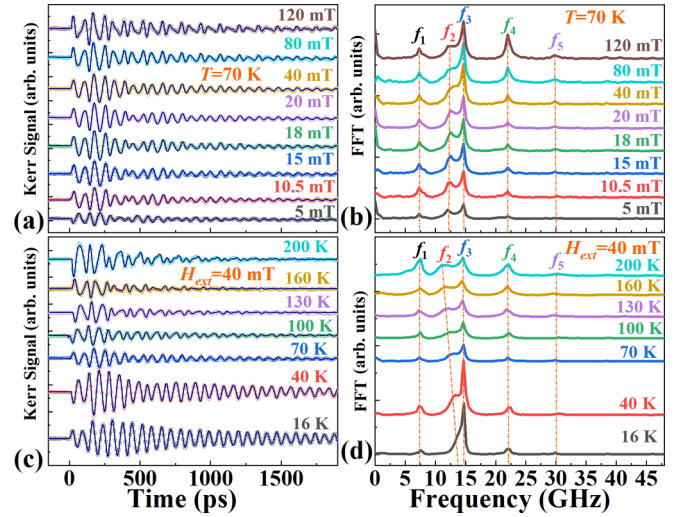

FIG. 2. (a) Typical experimental TR-MOKE signal measured at different external magnetic fields H_{ext} and constant temperature $T = 70$ K and (b) corresponding FFT spectra of the time-resolved traces. (c) Typical experimental TR MOKE signal at different temperatures T and constant field $H_{ext} = 40$ mT and (d) corresponding FFT spectra of the time-resolved traces. All FFT spectra show five clear resonances at $f_1 = 7.4$ GHz, $f_2 = 12.8$ GHz, $f_3 = 14.7$ GHz, $f_4 = 22.3$ GHz, and $f_5 = 30.1$ GHz in both temperature and magnetic field-dependent measurements. The open dots and solid lines in (a,c) are the measured data and curves fitted with Eq. (1), respectively. The dashed lines in (b,d) are guides to the eye.

In order to analyze the transients in more detail, we fit the TR MOKE traces using a superposition of five oscillations [2,6]:

$$y(t) = \sum_{i=1}^{5} A_i e^{-\Gamma_i t} \sin\left(2\pi f_i t + \phi_i\right), \qquad (1)$$

where A_i, f_i, ϕ_i, and Γ_i are, respectively, the amplitude, frequency, initial phase, and damping rate characterizing the ith separate oscillation ($i = 1, 2, 3, 4,$ and 5) contributing to the overall MOKE signal. The choice of five oscillations in Eq. (1) is based on the number of resonances in the experimental FFT spectra.

Figure 3 displays the evolution of the oscillation frequencies f_i and the corresponding amplitudes A_i as a function of H_{ext} and T. It can be seen from Figs. 3(a) and 3(b) that except for the reduction of frequency f_2 with increasing T, the other frequencies remain constant within the 16–200 K temperature and 5–120 mT magnetic field intervals. Contrary to the rigidity of the *frequencies*, we found the *amplitudes* A_i to vary substantially, both with the increasing magnetic field and temperature. These changes in the amplitudes are summarized in Figs. 3(c) and 3(d). Figure 3(c) reveals that the amplitudes A_1, A_2, A_3, and A_5 as a function of H_{ext} show very similar behavior, first increasing for $H_{ext} < H_c$ and then remaining constant for $H_{ext} > H_c$. The amplitude A_4 is monotonically rising with increasing H_{ext}. Contrary to the H_{ext} dependence, in temperature dependence, all amplitudes A_i initially drop sharply for $T < 70$ K and remain approximately constant for $T > 70$ K. We note that the modes with the lowest and
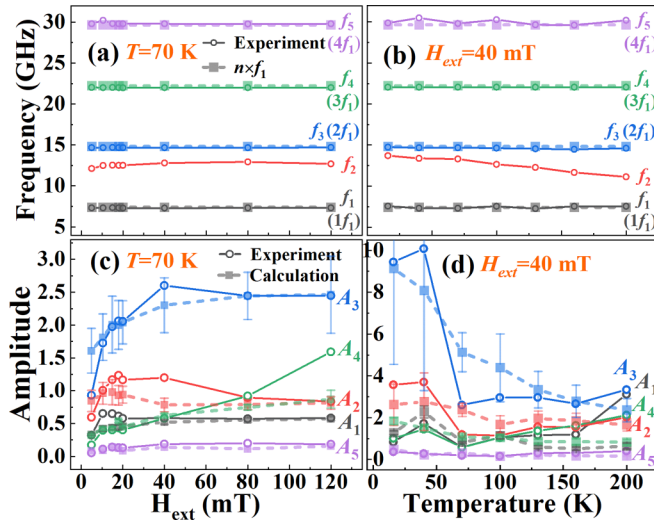
FIG. 3. Magnetic field dependence of (a) the oscillation frequencies f_i and (c) the oscillation amplitudes A_i measured at $T = 70$ K. Temperature dependence of (b) the frequencies f_i and (d) the oscillation amplitudes A_i measured at $H_{ext} = 40$ mT. The solid lines in (a,b) guide the eye and connect the experimental data points; the dashed lines mark the frequencies $f^{(n)}$ extracted from Eq. (2). The solid lines in (c,d) connect the experimental data points and the dashed lines are calculated using Eq. (4).

highest frequency almost disappear at $T = 16$ K, the lowest measured temperature. We observed the same tendencies at other temperatures and magnetic fields (see Figs. S1–S3 of the Supplemental Material [18]).

Figures 4(a)–4(e) and 4(f)–4(j) show the dependencies of the fitted damping rates Γ_i [see Eq. (1)] on the temperature T and magnetic field H_{ext}, measured at constant $H_{ext} = 40$ mT and $T = 70$ K, respectively. Additional results on the field and temperature dependencies of the damping rates at different constant T and H_{ext}, respectively, which corroborate the data

in Fig. 4 are compiled in Fig. S5 of the Supplemental Material [18]. From Figs. 4(a)–4(e) it can be seen that all damping rates increase with the different slopes as the temperature rises (also in Fig. S5 of the Supplemental Material [18]). There is no obvious dependence of the damping rates on the mode order. As for the magnetic field dependence (Figs. 4(f)–4(j) and Fig. S5 of the Supplemental Material [18]), the damping rates Γ_1, Γ_3, Γ_4, and Γ_5 are nearly independent of H_{ext}. Only Γ_2 increases with increasing magnetic field and is also the largest damping rate for all combinations of T and H_{ext} (Fig. 4 and Fig. S5 of the Supplemental Material [18]), which indicates a separate origin.

IV. DISCUSSION

Below we address three main aspects of our experimental findings, namely, (i) the fact that the frequencies of the superimposed oscillations (except f_2) are completely independent of T and H_{ext}, (ii) the trend of the oscillation amplitudes to decrease with increasing temperature and to weakly vary (increasing or decreasing) with increasing external magnetic field H_{ext}, and (iii) the observation that the damping rates (except for the f_2 mode) are independent of H_{ext}, but approximately linearly increase with T.

A. Rigidity of oscillation frequencies against magnetic field

The tunability of magnon resonant frequencies by external magnetic fields is an inherent signature of magnetization precession excited by an external trigger (e.g., magnetic field pulses, pulsed currents, spin-polarized currents, or ferromagnetic resonance (FMR) fields). The absence of this signature indicates a strong deviation from the expected standard behavior and indicates the presence of additional physical mechanisms impeding the tunability. Earlier publications on micro- and nanostructured ferromagnetic microstripes [22] and antidot lattices [23–25] indicate that the existence of field-independent magnonic modes can be associated with strong
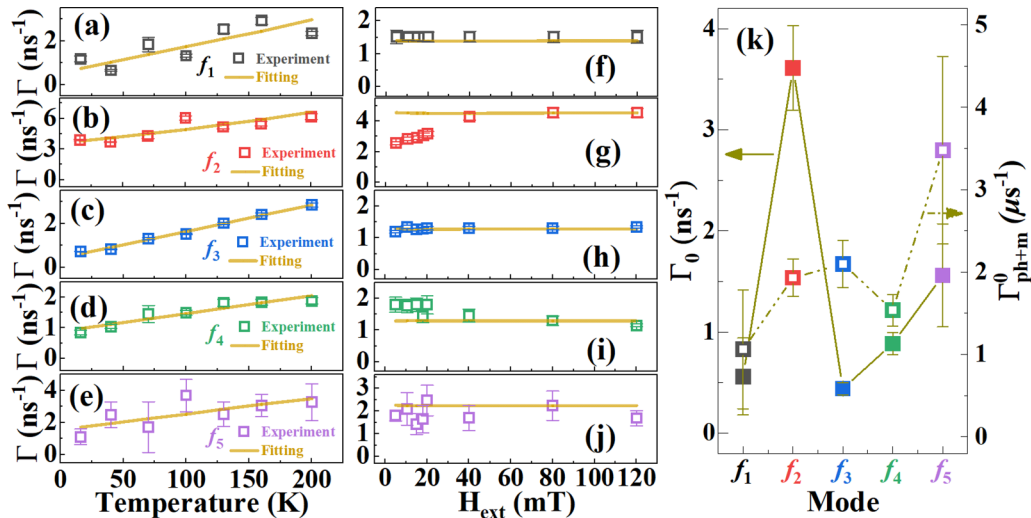

FIG. 4. (a–e) Temperature dependence of the damping rates Γ_i measured at the external magnetic field $H_{ext} = 40$ mT. (f–j) Magnetic field dependence of the damping rates Γ_i measured at the temperature $T = 70$ K. (a–j) The solid lines are fitted by Eqs. (6)–(8); see text. (k) Fitted elastic (Γ_0) and inelastic ($\Gamma_{ph}^0 + \Gamma_m^0$) damping rates of each mode.

demagnetizing fields at the edge of a specimen or with a nonuniform effective field profile in the sample. In addition, resonant frequencies weakly sensitive to the magnetic field have been ascribed to optically induced lattice-driven effects in Refs. [8,12,15,16,26]. In this work, we recorded oscillations in the GHz range in a laterally *continuous* magnetic multilayer with no artificially introduced lateral confinement (the only borders are introduced by the transmission line's lateral dimensions and the film thickness). Although the oscillations were recorded using a magnetization-sensitive technique—TR MOKE—the oscillation frequencies are magnetic field independent even at external magnetic fields exceeding the saturation field of the ferromagnetic layers. The latter observation indicates that the magnetic oscillations observed in this work are not inherent to the magnetic subsystem. We ascribe the observed frequencies to phononic oscillations.

In order to assess the viability of such an interpretation, we assume that in our Ag/Fe/Cr/Fe structures the ultrashort electromagnetic pulses cause an ultrafast magnetization transient via the torque that the external magnetic field pulse exerts on the magnetic moments of the Fe layers. We note that, in this work, we do not observe free magnetization precession triggered by the field pulse as was reported in earlier experiments on phonon-driven magnetization dynamics [13,15] or in magnetic pulse-driven dynamics [27,28]. According to our previous separate study of magnetization dynamics [29], this may be due to the large coercivity of our film, which suppresses the free magnetization precession. Nevertheless, the initial torque, which points normal to the sample plane, leads to a transient out of plane component of the magnetization. Since the magnetostrictive coefficient of Fe in <100> directions $\lambda_{100} = 2.1 \times 10^{-5}$ [30,31] is nonzero, the magnetoelastic coupling transduces the transient magnetization into a broad spectrum of phonons propagating normal to the sample plane. Due to the excellent epitaxy, these phonons easily propagate into the underlying Ag metallic buffer layer. Phonons that propagate normal to the sample plane and are reflected at the interfaces to the GaAs wafer and to the MgO cap layer can constructively interfere and form a standing sound wave. The wavelength of the fundamental wave fitting the total thickness $d = 161.9$ nm of the epitaxial Fe/Ag/Fe/Cr multilayer is much larger than the involved lattice constants. Therefore, the dispersion relation of the lowest-order acoustic modes is linear and can be written as

$$f^{(n)} = n \frac{v_s}{2d},\qquad(2)$$

where v_s is the longitudinal sound wave speed [12,16] and n the order of the particular oscillatory mode. Figure 5 shows the fit of Eq. (2) to the experimental frequencies f_1, f_3, f_4, and f_5 measured at $T = 70$ K and $H_{ext} = 40$ mT [Figs. 3(a) and 3(b)], which yields $v_s = 2.4 \pm 0.1$ km/s. This value is in good agreement with the speed of sound in Ag [32] which contributes most to the thickness of the metallic multilayer. The matching of the mode frequencies to the higher-order scheme is shown in Fig. S4 of the Supplemental Material [18] for measurements taken at other field and temperature combinations. Hence, the constructive interference of phonons triggered by the electromagnetic pulse leads to the formation of fundamental and corresponding higher-order long-living
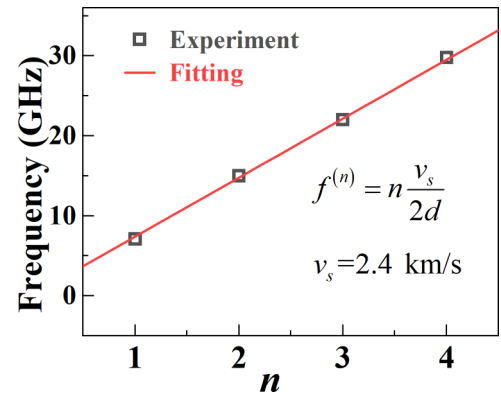

FIG. 5. Oscillation frequencies $f_i (i = 1, 3, 4, 5)$ measured at $T = 70$ K and $H_{ext} = 40$ mT versus mode order n. The solid line is a fit of the phonon dispersion relation in Eq. (2). The fitted slope $v_s = 2.4$ km/s is the longitudinal sound wave speed.

standing acoustic waves along the sample normal. The lattice oscillations, in turn, give rise to a periodic modulation of the orbital orientation and overlap in the Fe layers. As a consequence of such magnetoelastic coupling, the local magnetization, the magnetoelastic energy landscape (magnetoelastic anisotropy), and the exchange interaction between adjacent Fe sites may also be modulated and can drive parametrically coupled magnetization excitations [8] at the same frequencies as the phonon resonances. This reverse magnetoelastic effect of the magnetoelastic coupling thus results in the observed oscillating MOKE signal. Summarizing, we observe resonance frequencies of oscillations in the phonon subsystem, which are inherently independent of the magnetic field. The magnetic layers in our multilayer serve, first, as a transducer to convert the excitation field pulse into a force impulse acting on the lattice and, second, as a receiver of the high-frequency resonant lattice oscillations, which are converted into magnetization oscillations or periodic variations of the magneto-optic susceptibility detectable by MOKE.

We note that the mode giving rise to the frequency f_2 does not fit into the scheme of lattice-driven higher-order modes. Although the f_2 mode appears to coincide with the f_3 mode at the lowest temperature, it shows in contrast to all other observed modes a weak decrease of the frequency with increasing temperature [Figs. 2(d) and 3(b)]. There is also a significant decrease of the amplitude A_3, which is by far the largest at low temperature when the f_2 mode "splits off" as the temperature exceeds 40 K [See Figs. 2(d), 3(b), and 3(d)]. On the other hand, the f_2 mode is as independent of the external magnetic field as the other modes, which indicates a coupling to the phonon system. Nevertheless, the f_2 mode appears to have a somewhat different origin, but this has not been clarified yet.

B. Amplitude variation

The resonance amplitude of a driven harmonic oscillator is given by

$$A = \frac{F}{m\sqrt{\left(\omega^2 - \omega_0^2\right)^2 + \frac{\alpha^2 \omega_0^2}{m^2}}},\qquad(3)$$

where m is the mass of the iron atom; ω_0 is the natural frequency of the oscillation; $\alpha = \Gamma_i/\omega$ is the damping coefficient; and F is the driving force, which is related to the pulsed magnetic field strength, the effective magnetization, and the magnetoelastic coupling strength of the sample. It can be expected that F is different for each mode, and we will discuss this in the damping section. When the oscillator is in resonance, i.e., $\omega = \omega_0$, the resonant amplitude reaches maximum,

$$A_{\max}^{(n)}(H_{\text{ext}}, T) = \frac{F^{(n)}}{\alpha^{(n)}(H_{\text{ext}}, T)\omega_0^{(n)}(H_{\text{ext}}, T)}, \qquad (4)$$

and is inversely proportional to the damping coefficient. The maximum amplitudes according to Eq. (4) are plotted in Figs. 3(c) and 3(d) as squares connected by dashed lines. The amplitude values of each mode are obtained by inserting for $\alpha^{(n)}(H_{\text{ext}}, T)$ and $\omega^{(n)}(H_{\text{ext}}, T)$ in Eq. (4) the experimental values taken from Figs. 4 and 3(a), respectively. We note that the driving force $F^{(n)}$ varies strongly among the modes and is related to the magnetic field strength of the excitation pulse, the effective magnetization, and the magnetoelastic coupling strength of the sample. For example, for the field dependence of the experimental oscillation amplitudes [Fig. 3(c)], we observe that the oscillation amplitude increases when the magnetic field starts to increase from zero. This is due to the corresponding increase of the magnetization with the increasing field, which can be seen from the hysteresis loop in Fig. 1(d). Because of the absence of a quantitative understanding of the mode amplitudes measured by the Kerr effect, the strengths of the driving force $F^{(n)}$ were chosen so that they match the data in Figs. 3(c) and 3(d). Here, for the field dependence of the oscillation amplitudes [Fig. 3(c)], the values of the driving force $F^{(n)}$ are $F^1 = 0.87 \, \text{ns}^{-1}$, $F^2 = 3.2 \, \text{ns}^{-1}$, $F^3 = 2.6 \, \text{ns}^{-1}$, $F^4 = 1.0 \, \text{ns}^{-1}$, and $F^5 = 0.26 \, \text{ns}^{-1}$, respectively. For the temperature dependence of the oscillation amplitudes [Fig. 3(d)], the values of the driving force $F^{(n)}$ are $F^1 = 1.5 \, \text{ns}^{-1}$, $F^2 = 10.2 \, \text{ns}^{-1}$, $F^3 = 6.69 \, \text{ns}^{-1}$, $F^4 = 1.56 \, \text{ns}^{-1}$, and $F^5 = 0.54 \, \text{ns}^{-1}$, respectively. We note that Eq. (4) reproduces the tendency of the field and temperature dependencies of the mode amplitudes for each mode separately, but does *not* explain the relative amplitudes of the modes. The calculated results show trends similar to the experimental data, corroborating our interpretation that the observed oscillations originate from coherent phonons.

C. Damping behavior

Now we draw attention to the damping of the observed oscillations. In a recent theoretical study [16] on the damping of magnetization precession at a frequency $\omega = 2\pi f$ by phonon pumping into an adjacent metallic layer the magnetoelastic damping coefficient $\alpha_{me} = \Gamma/\omega$ was calculated. For an in-plane magnetized film the dependence on the external field is given by a factor

$$\alpha_{me} \propto \frac{\omega_H}{2\omega_H - \omega_A}, \qquad (5)$$

where $\omega_H = \gamma\mu_0 H_{\text{ext}}$ and $\omega_A = \gamma[(2K_1/M_s) - \mu_0 M_s]$ with γ being the gyromagnetic ratio, K_1 the magnetocrystalline anisotropy constant, and M_s the saturation magnetization.

Equation (5) predicts for Fe ($2K_1/M_s = 80 \, \text{mT}$, $\mu_0 M_s \approx 2 \, \text{T}$) in the field range from $H_{\text{ext}} = 5$ to $120 \, \text{mT}$ an approximately linear 20-fold increase of α_{me}. This is in clear contradiction with our results. Therefore, we conclude that the phonon pumping discussed in Ref. [16] is not the dominant damping mechanism in our system, which corroborates our interpretation above that the observed oscillations originate from coherent phonons that manifest as a magnetic signal only due to magnetoelastic coupling.

Experimental studies of systems with optically excited coherent magnons and phonons [6,8,26] have demonstrated that the damping behavior is related to the magnetic order [6] or even that the temperature dependence of the phonon oscillation amplitudes follows that of the magnetic order parameter [8]. The detailed analysis of the magnon-enhanced phonon damping in Ref. [6] considers three damping contributions with different temperature dependencies,

$$\Gamma(T) = \Gamma_0 + \Gamma_{\text{ph}}(T) + \Gamma_m(T), \qquad (6)$$

$$\Gamma_{\text{ph}}(T) = \Gamma_{\text{ph}}^0\left(1 + \frac{2}{e^{\frac{\hbar\omega}{2kT}} - 1}\right), \qquad (7)$$

$$\Gamma_m(T) = \Gamma_m^0\left(1 + \frac{2}{e^{\frac{\hbar\omega}{2kT}} - 1}\right)m(T), \qquad (8)$$

where Γ_0 is the damping (dephasing) due to elastic scattering of coherent phonons with defects, electrons, and incoherent phonons. Γ_0 is temperature independent if the excitation density (the laser fluence in Ref. [6], excitation magnetic field pulse in this work) is kept constant for each mode while the temperature is varied. $\Gamma_{\text{ph}}(T)$ is the contribution due to inelastic phonon-phonon scattering, and $\Gamma_m(T)$ is due to magnetoelastic coupling, which couples the lattice dynamics to excitations of the spin subsystem (phonon-magnon scattering) [6] with $m(T) = M(T)/M_s$ being the temperature dependence of the reduced magnetization. In Ref. [6], fitting Eqs. (6)–(8) to the experimental data could reproduce the temperature dependence magnon-enhanced phonon damping at Gd (0001) and Tb (0001) surfaces and reveals that the magnetoelastic contribution dominates until close to the Curie temperature. The data in Ref. [6] also show that at low temperature the oscillation amplitude is larger and the damping smaller, similar to this work.

Therefore, we use Eqs. (6)–(8) to fit the measured H_{ext} and T dependencies of the damping rates Γ_i shown in Fig. 4. For our measurement temperatures $T \ll T_c$ (for Fe $T_c = 1043 \, \text{K}$), the $m(T)$ dependence in Eq. (8) is very weak ($m = 1$ in our fitting) and thus does not allow us to separate the contributions from inelastic phonon-phonon [Eq. (7)] and phonon-magnon [Eq. (8)] scattering. In the framework of the model of Ref. [6], $T \ll T_c$ also explains the observed field independence of the damping rates. Considering that $\hbar\omega \ll kT$ and $m(T) = 1$ hold for our experiments, Eqs. (6) is linear in T to a good approximation with the y-axis intercept given by $\Gamma_0 + (\Gamma_{\text{ph}}^0 + \Gamma_m^0)$ and the slope by $(4k/\hbar\omega)(\Gamma_{\text{ph}}^0 + \Gamma_m^0)$. Therefore, we obtain from the fits for each mode the parameters Γ_0 and $\Gamma_{ph+m}^0 = \Gamma_{\text{ph}}^0 + \Gamma_m^0$. We note that the obtained values of Γ_0 and Γ_{ph+m}^0 are same for the field- and temperature-dependent measurements. The fitted Γ_0 and Γ_{ph+m}^0 values are plotted in Fig. 4(k).

It appears that Γ_0 increases for the four higher-order modes (f_1, f_3, f_4, and f_5) with the order number, indicating that the contribution from scattering with defects, electrons, and incoherent phonons is enhanced for higher-order modes. We note that the f_2 mode again does not fit into the higher-order scheme, confirming a different origin as mentioned before. Interestingly, the Γ^0_{ph+m} values of all modes turn out to be of the same order of magnitude of $1\,\mu s^{-1}$ and thus are about two to three orders of magnitude smaller than Γ_0. The different slopes in Figs. 4(a)–4(e) are mainly due to the different mode frequencies. The comparison of the calculated and experimental data shows good agreement for the temperature dependence, but it seems there are some deviations for the field dependence. We suspect that these deviations may be related to microscopic inhomogeneities of the magnetization that have a different impact on the different resonant modes. Further experiments are needed to clarify this issue.

V. CONCLUSION

We magneto-optically detected high-order lattice oscillations in Ag/Fe/Cr/Fe films patterned into a long coplanar transmission line. The oscillation frequencies are independent of temperature (16–300 K) and magnetic field (up to 120 mT) variations. We ascribe the presence of these very rigid high-frequency phonons to strong magnetoelastic coupling between the lattice and magnetization subsystems. The magnetic layers in the multilayer serve as a transducer to convert the exciting ultrafast electromagnetic field pulse into a force impulse acting on the lattice. Once the long-lived (ns) lattice oscillations are excited, the magnetic trilayer also acts as a receiver and converts, again via magnetoelastic coupling, the high-frequency resonant lattice oscillations into magnetization oscillations detectable by MOKE. The assignment of the detected magnetization oscillations to a phononic origin is corroborated by the field and temperature dependencies of the oscillation damping rates and amplitudes. The coherent lattice oscillations are acoustic phonons that propagate in the direction normal to the sample plane, are reflected at the interfaces to the substrate and the vacuum, and constructively interfere to form standing sound waves. The frequency of the coherent phonons shows excellent field and temperature stability, and their damping rate linearly increases with temperature and is only weakly field dependent. This work shows a way of using magnetoelastic coupling to achieve higher-order phonon oscillations. We expect that this analysis will contribute to a detailed understanding of coupling between lattice and magnetic subsystems, potentially opening a path of their mutual control for energy efficient and magnetic field-resistant high-frequency applications.

[1] A. Kirilyuk, A. V. Kimel, and T. Rasing, Rev. Mod. Phys. **82**, 2731 (2010).

[2] M. Deb, E. Popova, M. Hehn, N. Keller, S. Petit-Watelot, M. Bargheer, S. Mangin, and G. Malinowski, Phys. Rev. Lett. **123**, 027202 (2019).

[3] V. N. Kats, T. L. Linnik, A. S. Salasyuk, A. W. Rushforth, M. Wang, P. Wadley, A. V. Akimov, S. A. Cavill, V. Holy, A. M. Kalashnikova, and A. V. Scherbakov, Phys. Rev. B **93**, 214422 (2016).

[4] B. Koopmans, G. Malinowski, F. Dalla Longa, D. Steiauf, M. Fähnle, T. Roth, M. Cinchetti, and M. Aeschlimann, Nat. Mater. **9**, 259 (2010).

[5] E. Beaurepaire, J. C. Merle, A. Daunois, and J. Y. Bigot, Phys. Rev. Lett. **76**, 4250 (1996).

[6] A. Melnikov, A. Povolotskiy, and U. Bovensiepen, Phys. Rev. Lett. **100**, 247401 (2008).

[7] C.-H. Lambert, S. Mangin, B. S. D. C. S. Varaprasad, Y. K. Takahashi, M. Hehn, M. Cinchetti, G. Malinowski, K. Hono, Y. Fainman, M. Aeschlimann, and E. E. Fullerton, Science **345**, 1337 (2014).

[8] A. Melnikov, I. Radu, U. Bovensiepen, O. Krupin, K. Starke, E. Matthias, and M. Wolf, Phys. Rev. Lett. **91**, 227403 (2003).

[9] K. Chen and S. Zhang, Phys. Rev. Lett. **114**, 126602 (2015).

[10] S.-h. C. Baek, V. P. Amin, Y.-W. Oh, G. Go, S.-J. Lee, G.-H. Lee, K.-J. Kim, M. D. Stiles, B.-G. Park, and K.-J. Lee, Nat. Mater. **17**, 509 (2018).

[11] C. Dornes, Y. Acremann, M. Savoini, M. Kubli, M. J. Neugebauer, E. Abreu, L. Huber, G. Lantz, C. A. F. Vaz, H. Lemke, E. M. Bothschafter, M. Porer, V. Esposito, L. Rettig, M. Buzzi, A. Alberca, Y. W. Windsor, P. Beaud, U. Staub, D. Zhu *et al.*, Nature (London, U. K.) **565**, 209 (2019).

[12] D. Afanasiev, I. Razdolski, K. M. Skibinsky, D. Bolotin, S. V. Yagupov, M. B. Strugatsky, A. Kirilyuk, T. Rasing, and A. V. Kimel, Phys. Rev. Lett. **112**, 147403 (2014).

[13] A. S. Salasyuk, A. V. Rudkovskaya, A. P. Danilov, B. A. Glavin, S. M. Kukhtaruk, M. Wang, A. W. Rushforth, P. A. Nekludova, S. V. Sokolov, A. A. Elistratov, D. R. Yakovlev, M. Bayer, A. V. Akimov, and A. V. Scherbakov, Phys. Rev. B **97**, 060404(R) (2018).

[14] A. V. Scherbakov, A. S. Salasyuk, A. V. Akimov, X. Liu, M. Bombeck, C. Brüggemann, D. R. Yakovlev, V. F. Sapega, J. K. Furdyna, and M. Bayer, Phys. Rev. Lett. **105**, 117204 (2010).

[15] J. V. Jäger, A. V. Scherbakov, B. A. Glavin, A. S. Salasyuk, R. P. Campion, A. W. Rushforth, D. R. Yakovlev, A. V. Akimov, and M. Bayer, Phys. Rev. B **92**, 020404(R) (2015).

[16] S. Streib, H. Keshtgar, and G. E. W. Bauer, Phys. Rev. Lett. **121**, 027202 (2018).

[17] D. E. Bürgler, C. M. Schmidt, D. M. Schaller, F. Meisinger, R. Hofer, and H. J. Güntherodt, Phys. Rev. B **56**, 4149 (1997).

[18] See Supplemental Material at http://link.aps.org/supplemental/10.1103/PhysRevB.104.054430 for the measured picosecond current pulse generated by the LT GaAs photoconductive switch, and the data (TR MOKE signal, oscillation frequencies, oscillation amplitudes, and damping rate) of other temperature and magnetic field dependent results.

[19] R. Adam, M. Mikulics, A. Förster, J. Schelten, M. Siegel, P. Kordoš, X. Zheng, S. Wu, and R. Sobolewski, Appl. Phys. Lett. **81**, 3485 (2002).

[20] M. Mikulics, R. Adam, Z. Sofer, H. Hardtgegen, S. Stanček, J. Knobbe, M. Kočan, J. Stejskal, D. Sedmidubský, M. Pavlovič, V. Nečas, D. Grützmacher, and M. Marso, Semicond. Sci. Technol. **25**, 075001 (2010).

[21] C. M. Schmidt, D. E. Bürgler, D. M. Schaller, F. Meisinger, and H. J. Güntherodt, Phys. Rev. B **60**, 4158 (1999).

[22] M. Bailleul, D. Olligs, and C. Fermon, Phys. Rev. Lett. **91**, 137204 (2003).

[23] H. Ulrichs, B. Lenk, and M. Münzenberg, Appl. Phys. Lett. **97**, 092506 (2010).

[24] S. Neusser, B. Botters, and D. Grundler, Phys. Rev. B **78**, 054406 (2008).

[25] S. Neusser, G. Duerr, H. G. Bauer, S. Tacchi, M. Madami, G. Woltersdorf, G. Gubbiotti, C. H. Back, and D. Grundler, Phys. Rev. Lett. **105**, 067208 (2010).

[26] A. M. Kalashnikova, A. V. Kimel, R. V. Pisarev, V. N. Gridnev, P. A. Usachev, A. Kirilyuk, and T. Rasing, Phys. Rev. B **78**, 104301 (2008).

[27] A. A. Rzhevsky, B. B. Krichevtsov, D. E. Bürgler, and C. M. Schneider, Phys. Rev. B **75**, 224434 (2007).

[28] T. Gerrits, J. Hohlfeld, O. Gielkens, K. J. Veenstra, K. Bal, T. Rasing, and H. A. M. van den Berg, J. Appl. Phys. **89**, 7648 (2001).

[29] D. Cao, X. Cheng, L. Pan, H. Feng, X. Cheng, C. Zhao, Z. Zhu, Q. Li, J. Xu, S. Li, Q. Liu, and J. Wang, AIP Adv. **7**, 115009 (2017).

[30] L. Daniel, O. Hubert, and R. Billardon, Comput. Appl. Math. **23**, 285 (2004).

[31] L. Daniel and O. Hubert, Eur. Phys J.: Appl. Phys. **45**, 31101 (2009).

[32] P. Ji and Y. Zhang, Appl. Phys. A **123**, 671 (2017).